Analyzing the IAR with IRI During the Recent Solar Minimum

S. Ivanov[1], J. Klenzing[2], F. Simões[3]
NASA, Goddard Space Flight Center, Greenbelt, Maryland, 20770

The 2008-2009 solar minimum was deeper than any within the past century. As such, the performance of the empirical International Reference Ionosphere (IRI) model was impacted. This impact manifested as a disagreement between predicted and measured characteristic separation in frequency for a wave resonating within an Ionospheric Alfvén Resonator (IAR). The predicted value of the characteristic was a factor of three lower than what was measured by the Communication/Navigation Outage Forecast System (C/NOFS). Analyzing the model performance and comparing output with measured ionospheric values showed that more than half of the inaccuracy could be explained by inaccuracies in the output of the model. The 2008-2009 solar minimum was outside of the bounds of the effectiveness of the empirical IRI model. Incorporating recent data measurements and new indices would increase the accuracy of IRI during this period.

Nomenclature

B_r = radial component of the Earth's magnetic field
μ_0 = constant of permeability
ρ = density
ω = the frequency of an Alfvén wave
ε = the ratio of the minimum Alfvén velocity to the maximum Alfvén in a specific electron density profile
H = the characteristic height of an IAR
L = the characteristic length of an IAR
V_a = the Alfvén velocity
Δf = the characteristic separation in frequency between two Alfvén waves in an IAR

I. Introduction

A. Alfvén Waves

Alfvén waves are a type of magnetohydrodynamic wave which can form and propagate in a magnetized plasma. It occurs when a plasma is suffused with a magnetic field. Perturbations to plasma homogeneity which displace ions within the plasma can occur, as a result, owing to the internal magnetic field, a magnetic restoration force is exerted on the displaced ions, moving them back into equilibrium. The result is a wave which travels along the magnetic field lines inside the plasma and displaces amplitude transverse to its motion vector. The velocity of an Alfvén wave is a function of the ambient density and the strength of the magnetic field permeating the plasma (Ref. 1).

$$V_a = \frac{B_r}{\sqrt{\mu_0 \rho}}$$

B. IAR

The ionospheric Alfvén resonator is a local structure which may form in the Earth's ionosphere between the lower bound of the ionosphere and the lower bound of the magnetosphere. The existence, or lack thereof, of an IAR is based on the local ionospheric properties. For an IAR to form, a cavity with two reflective surfaces is required to form, with each surface being normal to a component of the Earth's magnetic field.

[1]NASA USRP intern, Georgia Institute of Technology, sivanov3@mail.gatech.edu

[2]Postdoctoral Fellow, Space Weather Laboratory, Heliophysics Science Division, NASA Goddard, Code 674
[3]Postdoctoral Fellow, Space Weather Laboratory, Heliophysics Science Division, NASA Goddard, Code 674
An IAR will form along the radial components of the Earth's magnetic field, and as such they don't exist over the geomagnetic equator. The lower bound of the ionosphere is usually considered reflective, since there is a sufficiently sharp gradient when the ionosphere begins that this boundary is almost always reflective to Alfvén waves (Ref. 1, 8).

Figure 1 illustrates the electron density profile, the Alfvén velocity profile and the index of refraction profiles which would yield an IAR. The characteristic depth, ε, of the IAR is the minimum Alfvén velocity divided by the maximum. L is the length of the resonator and H is the scale height, calculated from the slope of the upper Alfvén velocity curve. The upper boundary of the resonator must meet a number of conditions in order to provide wave reflection. There must be a sufficiently sharp gradient in the index of refraction in order for there to exist an upper boundary to the resonator.

Figure 1

Furthermore, the medium must meet the transparency condition detailed by:

$$\pi\varepsilon\omega H/V_a$$

Where ε is the ratio of the minimum Alfvén velocity over the maximum Alfvén velocity over the altitude range of interest and ω is the frequency of the wave. Ideally, the medium within the cavity should be transparent to an Alfvén wave but the upper and lower boundaries should be opaque, otherwise the wave would escape to the ground or out into space. Alfvén waves trapped inside an IAR have been detected on the ground because the lower boundary is not a perfect reflector. In figure 1, an IAR exists between 100 and 300 kilometers.

C. Ionospheric Measurements

Data regarding ionospheric parameters can be gathered either with ground based instruments or with space based observatories. Ground based observatories (ionosondes) can project radio waves into the ionosphere and analyze those reflected. By varying the frequency of the projected waves they can calculate the electron densities in the ionosphere, since the reflectivity of the ionosphere to certain waves is related to the wave's frequency and the electron density in the ionospheric plasma. Waves below a critical frequency will be reflected by regions of the ionosphere while waves of or above the critical frequency will treat the regions as transparent. Thus, by varying the frequency of the broadcast waves ground stations can calculate both the electron densities in the ionosphere as well as the altitude of the F peak. The F peak is the altitude of maximum electron density. This, however, is the extent of ground-based measurements, they can only provide bottom-side measurements of the ionospheric parameters (Ref. 3).

Satellites and other space-based observatories observe the ionosphere from above the F peak. These orbital observatories provide topside measurements of ionospheric conditions.

D. C/NOFS

C/NOFS is the first spacecraft to detect IAR signatures in space. Using the Vector Electric Field Instrument (VEFI) on board the satellite, C/NOFS was able to detect Alfvén waves resonating inside an IAR. Many IAR signatures have thus far been detected, identifiable by their unique 'footprint' in the frequencies measured by the satellite instruments, shown in figure 2 (Ref. 4).

Figure 2 (IAR footprint)

They were characterized using the difference in frequency between two consecutive peaks. When these observations were compared to expectations produced by model output, they showed significant disagreement. The characteristic separation in frequency, Δf , calculated from the IRI output was smaller by a factor of three or four than what was observed with VEFI. The difference between consecutive peaks can be derived from

$$\Delta f = \frac{V_a}{2(L+H)}$$

IRI has a history of overestimating electron densities in the ionosphere during the recent solar minimum. Such an overestimation would dampen the predicted Δf and produce a disagreement with VEFI measurements. Furthermore, the observations were made during the 2008-2009 solar minimum, which is the deepest minimum within the last century. Taking both of these features into account, an analysis of IRI performance was made in order to determine if the disagreement was due to model or IAR formulation issues (Ref. 6, 7, 9, 10).

E. Dataset

The C/NOFS mission has been operating for several years, producing useful data. This study analyzed data produced by C/NOFS starting September 8th, 2008 and ending October 2nd, 2010, covering the deep solar minimum and subsequent rise in solar activity. The Coupled Ion-Neutral Dynamics Investigation (CINDI) instrument suite on board C/NOFS produces measurements of the electron density and chemical composition (O+, He+, H+) roughly every half second, but this data was sampled at one minute intervals over the course of the dataset. The absolute electron density and the ion composition of the ionosphere were taken from the available dataset. Furthermore, each of the values had a time stamp and a measurement of the position of the satellite relative to the surface of the earth associated with it.

F. IRI Modeling

Testing the effectiveness of IRI required generating IRI predictions of the state of the ionosphere. Using the position and time information which accompanied every measurement of interest from C/NOFS, the IRI model was used to generate a prediction of plasma ionospheric conditions. This data was then compared with the C/NOFS measurements.

II. Comparisons

Three comparisons were made with the acquired data. First, a ratio of the square root of the IRI density prediction divided by the C/NOFS measured density. Second, a ratio of the square root of the IRI average mass divided by the C/NOFS average mass, i.e. a sum of the ion masses multiplied by their normalized abundance. And finally a composite ratio of the Alfvén velocity calculated from the C/NOFS measurements divided by the Alfvén velocity calculated from IRI predictions. IRI consistently overestimates the electron densities in the topside ionosphere, so ratios greater than one were expected. A larger ratio means a greater inaccuracy of the IRI model, however it also means that more of the discrepancy between the IRI predicted Δf and the C/NOFS measured Δf is explained by inaccuracies in the IRI predictions.

The ratios were averaged over the course of an entire day and then plotted over the course of the mission. This comparison was extended further into daytime averages and nighttime averages. That is, the day-averages were split into portions where the satellite was observing the ionosphere that was in sunlight and where it was observing the ionosphere in darkness. This was done because the IAR is more likely to form during the night than during the day[1].

III. Results

A. Electron Density

The electron density ratio for the whole-day average ratios showed an average value of 1.32 over the course of the mission. However, when the ratios were split into daytime and nighttime values the daytime ratios were larger in magnitude, around 1.33, whereas the nighttime ratios were close to 1.29.

B. Average Mass

The average mass is a measure of the average mass in the ionosphere created from IRI predictions of chemical composition and C/NOFS measurements of charged ions. On average, the output of IRI was more accurate in terms of the average mass, producing an overall mission value of 1.26, smaller than the average inaccuracy in the electron density for the whole-day average ratios. However, when the values were split into daytime and nighttime ratios, the nighttime predictions were significantly more inaccurate than the daytime predictions. Daytime predictions averaged

1 See Appendix section C.

a ration of around 1.20 over the course of the whole mission whereas nighttime ratios averaged 1.40.

C. Alfvén Velocity

The final comparison was the composite ratio of the Alfvén velocity. This comparison was the most important since the Δf measurements vary as a function of the Alfvén velocity. The whole-day ratios averaged, over the course of the mission, a ratio of 1.65. The daytime and nighttime ratio averages were again significantly different from each other. The daytime mission-wide average was around 1.59 whereas the nighttime mission-wide average was just above 1.76.

Ratios of (IRI)/(C/NOFS)	All Day	Daytime	Nighttime
Electron Density (All mission)	1.3257	1.3327	1.2919
Average Mass (All mission)	1.2679	1.2017	1.4037
Alfvén Velocity (All mission)	1.6474	1.5907	1.7605
Electron Density (0-400 days)	1.3696	1.3804	1.3214
Average Mass (0-400 days)	1.3842	1.2938	1.5708
Alfvén Velocity (0-400 days)	1.8353	1.7597	1.9889
Electron Density (400 days-end)	1.2795	1.2824	1.2614
Average Mass (400 days-end)	1.1452	1.1049	1.2265
Alfvén Velocity (400 days-end)	1.4495	1.4130	1.5193

Table 1: The table contains the average ratios for the quantities of interest, Electron density, Average mass and Alfvén velocity ratios, over the course of the whole mission, as well as pre-day 400 and post-day 400, split into whole day averages and daytime and nighttime averages.

D. Solar Activity Transition

Plotting the ratios also produced another interesting result. The accuracy of the IRI model increased after day 400 of the analysis. Prior to day 400, when solar activity was still in the minimum, the ratios were higher, thus indicating greater inaccuracy, and also displayed a greater variability in the predictions. However, after day 400, when solar activity begins to rise, IRI predictions improve. The ratios decrease, though they are still significant, and the variability in the predictions likewise decreases.

To illustrate, prior to day 400, the whole-day averages for the electron density, average mass and Alfvén velocity ratios were 1.36, 1.38 and 1.83 respectively. After day 400, they were 1.27, 1.14 and 1.45. As solar activity increased, and as the solar indices moved out of their plateau regions, the accuracy of IRI increased markedly. Figures 3-5 contain the ratio plots and illustrate the trends mentioned here. The line at day 400 marks the beginning of the transition out of solar minimum and the increased accuracy of the model.

Figures 3-5 (Ratio Plots)

E. Solar Indices and IRI

IRI uses, among other parameters, a set of solar indices to determine the affects of solar radiation on the ionosphere. The two main indices investigated in the study are the RZ sunspot number (a measure of the number of sunspots on the surface of the sun) and the IG monthly average values (from the UK Solar System Data Centre). Both of these indices are used for historical reasons. The RZ sunspot number is available since Galileo, whereas the IG parameter, which is a global-average bottom-side measurement, stretches back decades. More recent and, it can be said, more accurate, indices have existed only for a few years and at most decades, thus limiting the amount of empirical data available to correlate with them (Ref. 2).

These indices are used as proxies to derive the actual solar output and thus play a role in producing the predictions of IRI. However, the RZ index shows a plateau during the solar minimum, and the IG, which is calculated monthly, would dampen the effects day-to-day variations in solar output. The RZ value bottoms out at 0 and stays in that vicinity over the course of the solar minimum. However, even as the RZ value reaches its minimum, solar activity

continued to decline to the absolute solar minimum. As discussed before, once solar activity transitions from the solar minimum, IRI begins producing better predictions. As this transition occurs, the RZ index begins to increase, indicating that IRI inaccuracy is connected to the sensitivity of the RZ index.

Figures 6 and 7 IG and RZ

Further comparisons were made between these indices used by IRI and other possible measurements of solar activity including the Magnesium 2 (wavelength of 280 nanometers) solar index, the Lyman Alpha (wavelength of 122 nanometers) index and the integrated solar flux between 17 and 91 nanometers (the range of EUV radiation which is absorbed by the region of the ionosphere of interest). All of these measurements showed a similar behavior. As solar activity decreases, these values approach a plateau and do not convey the entire behavior of solar output during the solar minimum (Ref. 5).

Figures 8-10 Lyman Alpha, EUV, Magnesium 2

IV. Discussion

A. IRI and the Solar Minimum

The disagreement between the predicted Δf and the measured Δf was a result, in part, of the inaccuracies of the IRI predictions made during the solar minimum. These inaccuracies are likely the result of the extreme nature of the 2008-2009 solar minimum. The empirical model was not produced with measurements comparable to this minimum and as such reaches the limit of its effectiveness during this minimum. Incorporating the measurements made during this solar minimum into future versions of IRI would enhance its effectiveness both in the future and in data analysis during this 2008-2009 solar minimum.

B. IRI and Solar Indices

IRI uses the IG and RZ solar indices because of the historical availability of data associated with them. However, these indices proved to be of limited effectiveness in the 2008-2009 solar cycle where they reached an extended minimum value whereas the solar cycle was still moving into its absolute minimum. Several of the other solar indices, namely the Magnesium 2, the EUV flux for wavelengths between 17nm and 91nm and the Lyman Alpha indices showed similar behaviors, reaching a an extended minimum value whereas the solar output was still dropping to its minimum. The implementations of new indices in future versions of IRI would help prevent insensitivity in the indices during future deep solar minimums and would allow for better analysis of data using IRI during this solar minimum. Additionally, though the indices show the same general trend, plateau followed by rise during the transition from solar minimum, they show different variability patterns after the transition. Further work will have to be done to determine which single index, or combination of indices, serves as best activity index for future empirical topside models.

V. Conclusion

The inaccuracies of the IRI model during the 2008-2009 solar minimum resulted from the lack of previous observations of such a deep solar minimum. This limited the effectiveness of the empirical IRI model. Up to half of the discrepancy between measured delta f and observed delta f can be explained by this inaccuracy. Furthermore, incorporating the newly observed solar and ionospheric data into IRI and updating the solar indices used would increase the effectiveness of IRI during future deep solar minima and when analyzing data during the 2008-2009 solar minimum.

Appendix

A. Data Gathering

The C/NOFS data was available from the CINDI instrument suite at roughly half second intervals, though points were not always available. The data was sampled every 120 points from the data arrays, roughly every minute, over the course of the entire array.

B. Data Processing

The minute-interval data points were composed of electron density, chemical composition, altitude, latitude,

longitude and daytime information as well as a timestamp of the measurement. Using these measurements, predictions were generated with the IRI model. The observed data and the IRI predictions were then used to calculate a ratio, as specified earlier, of the electron densities, average mass and the Alfvén velocities. The minute-interval ratios were then initially averaged over the course of the day. They were later split up into daytime and nighttime values using the daytime information included with the observations, which stated whether or not the satellite was in sunlight. Once the values were split according to nighttime or daytime, they were averaged again to generate daily daytime and nighttime averages.

C. IAR Formation

Initial analysis of ionospheric electron profiles showed that the transparency conditions for the formation of an IAR over a likely range of Alfvén wave frequencies was more likely to occur during nighttime than during daytime. The reflectivity condition, especially during midday, was not met and an IAR would likely not have formed. However, during nighttime, the conditions were more suitable with both boundaries of the IAR likely to exist. This is why the averages were split into daytime and nighttime ratios.

Acknowledgments

CINDI data are provided through the auspices of the CINDI team at the University of Texas at Dallas supported by NASA grant NAS5-01068. TIMED/SEE data are provided courtesy of Laboratory for Atmospheric and Space Physics at the University of Colorado. This project was supported by the NASA USRP internship program

References

[1]Belyaev, P. P., Polyakov, S. V., Rapoport, V. O., and Trakhtengerts, V. Yu., "The ionospheric Alfven resonator," *Journal of Atmospheric and Terrestrial Physics,* Vol. 52, No. 9, 1990, 781-788.

[2]Bilitza, D., "International Reference Ionosphere 2000," *Radio Science*, Vol. 36, No. 2, 261-275.

[3]Bösinger, T., Demekhov, A. G. and, Trakhtengerts, V. Y., "Fine structure in ionospheric Alfven resonator spectra observed at low latitude (L=1.3)," *Geophysical Research Letters*, Vol. 31, 2004, L18802.

[4]de La Beaujardiére, O. et al., "C/NOFS: a mission to forecast scintillations," *Journal of Atmospheric and Solar-Terrestrial Physics,* Vol. 66, Sept. 14, 2004, 1573-1591.

[5]Garriot, O. K. and Rishbeth, H., *Introduction to Ionospheric Physics,*Academic Press, New York and London, 1969, pp. 106.

[6]Heelis, R. A. et al., "Behavior of the O+/H+ transition height during the extreme solar minimum of 2008," *Geophysical Research Letters,* Vol. 36, July 24, 2009, L00C03.

[7]Lühr, H. and Xiong, C., "IRI-2007 model overestimates electron density during the 23/24 solar minimum," *Geophysical Research Letters,* Vol. 37, 2010, L23101.

[8]Lysak, R. L., "Propagation of Alfven waves through the ionosphere: Dependence on ionospheric parameters," *Journal of Geophysical Research*, Vol. 104, No. A5, 1990, 10,017-10,030.

[9]Nsumei, P. A., Reinisch, B. W., Huand, X. and, Bilitza, D., "Comparing topside and bottomside-measured characteristics of the F2 layer peak," *Advances in Space Research,* Vol. 46, June, 2010, 874-983.

[10]Potula, B. S., Chu, Y., Uma, G., Hsia, H. and, Wu, K.,"A global comparative study on the ionospheric measurements between COSMIC radio occultation technique and IRI model," *Journal of Geophysical Research,* Vol. 116, 2011, A02310.

Figures:

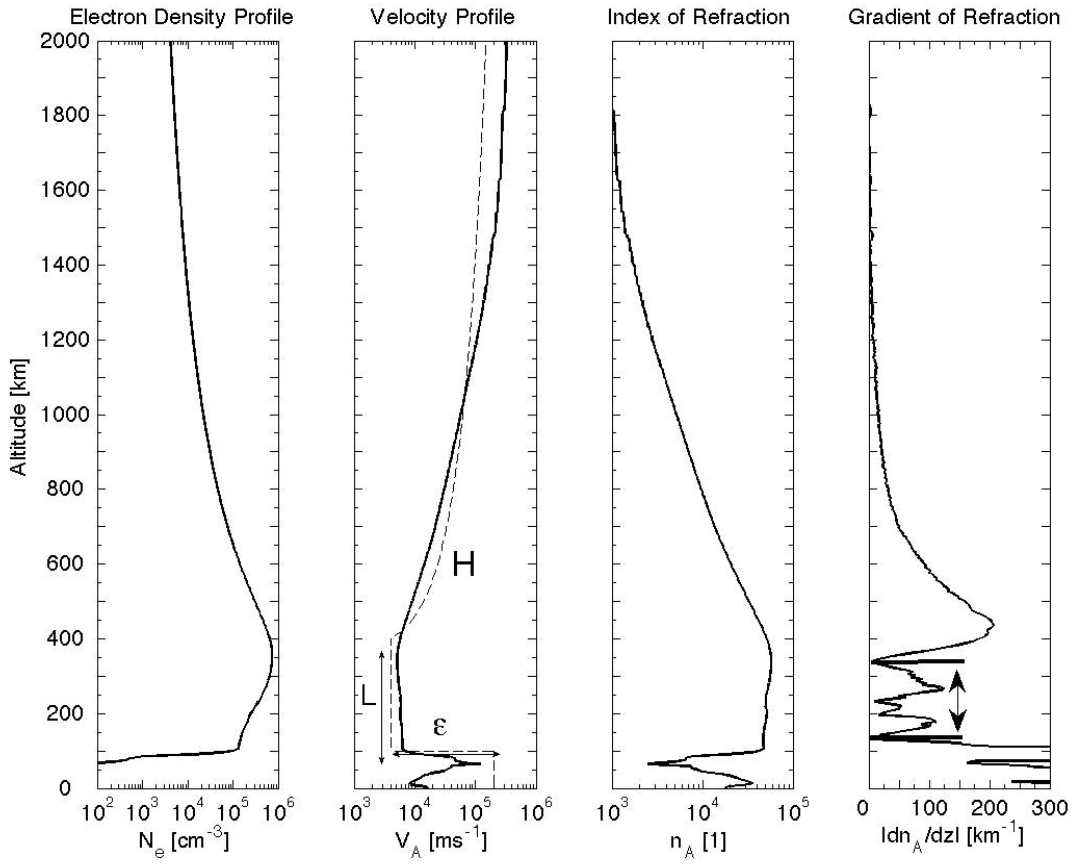

Figure 1: The figure shows an ionospheric profile which forms an IAR. The electron density profile (panel 1, from left) peaks at the F peak and then declines with altitude. This profile creates an Alfvén velocity profile (panel 2) with a similar jump in magnitude where electron density is low and a drop where electron density is high. The characteristics of the Alfvén velocity profile of interest are the length of the resonator, L, the characteristic height of the velocity profile, H, and the depth of the profile, ε. Panel 3 shows the Alfvén refraction index, n_A. The gradient of the index of refraction (panel 4) shows two sharp jumps at 100 km and 300 km altitude; these are the two boundaries of the resonator.

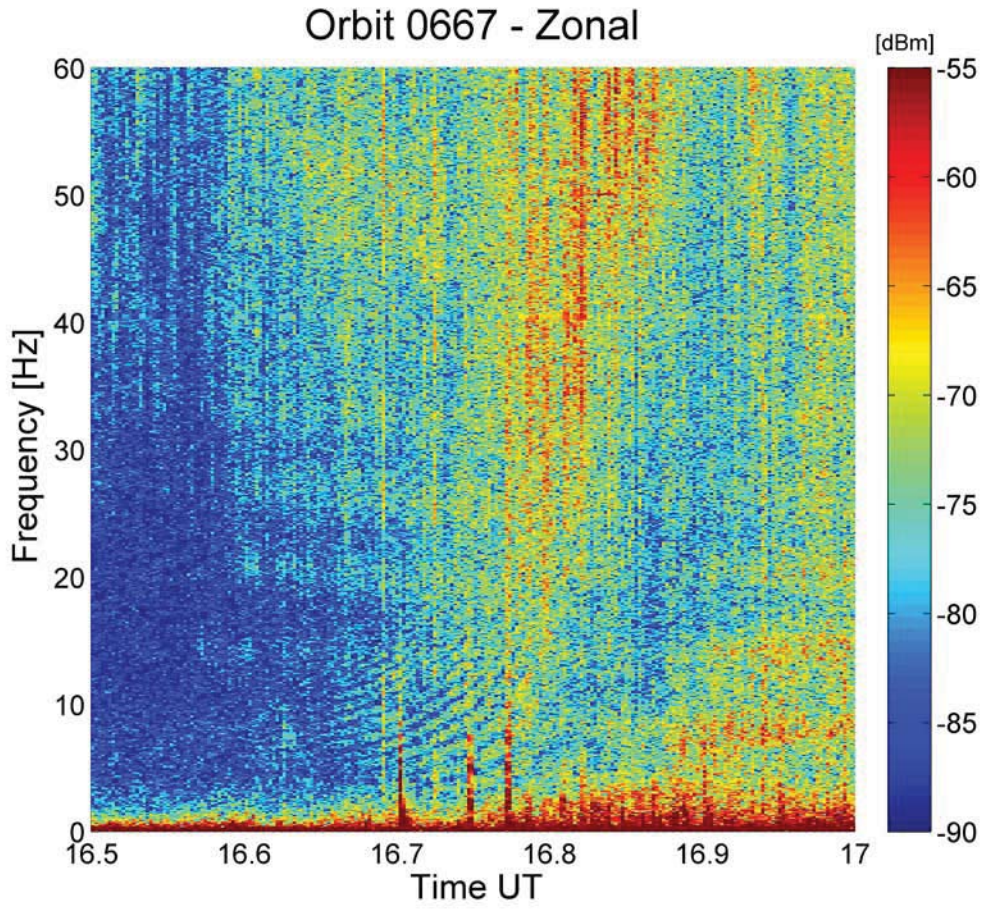

Figure 2: The figure shows a footprint of an IAR measured by C/NOFS on May 31, 2008. The signature is present in the range 2-15 Hz at 16.65-16.75 UT. The characteristic separation in frequency, Δf, is calculated from the difference between two consecutive peaks measured here.

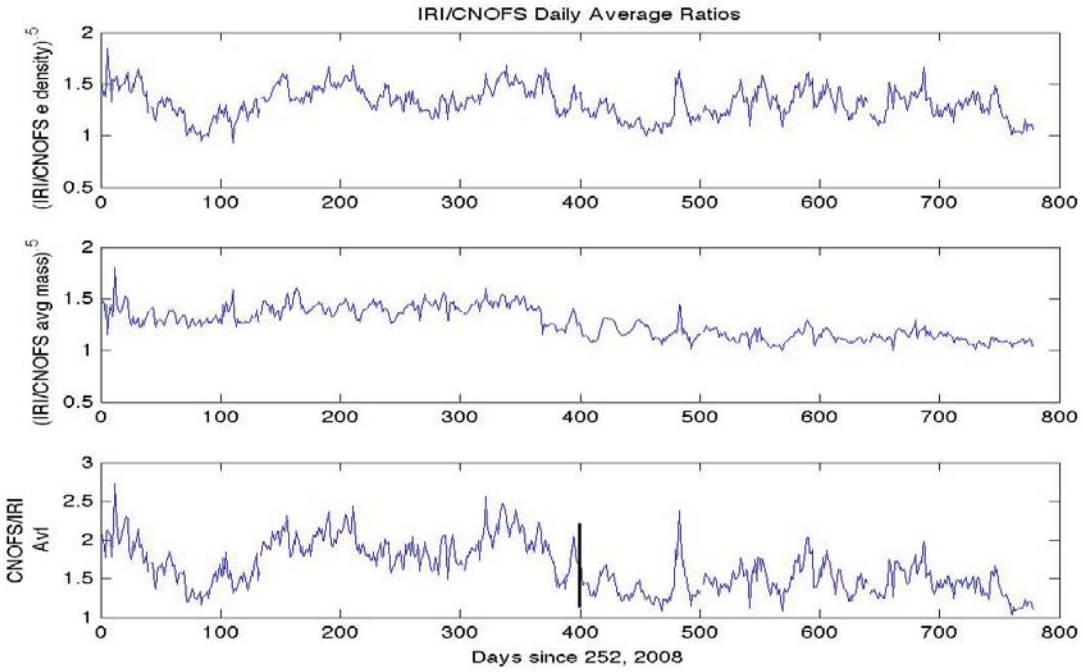

Illustration 3: The figure shows daily ratios over the course of the mission – from top, the square root of the ratio of the IRI electron density to the C/NOFS measurements, the square root of the ratio of average mass (ion mass multiplied by fraction of atmospheric composition) of IRI to C/NOFS measurements, and the ratio of average Alfvén velocity of IRI to C/NOFS. The transition out of solar minimum can be seen at day 400. It is very clear in the Alfvén velocity ratio and in the average mass ratio.

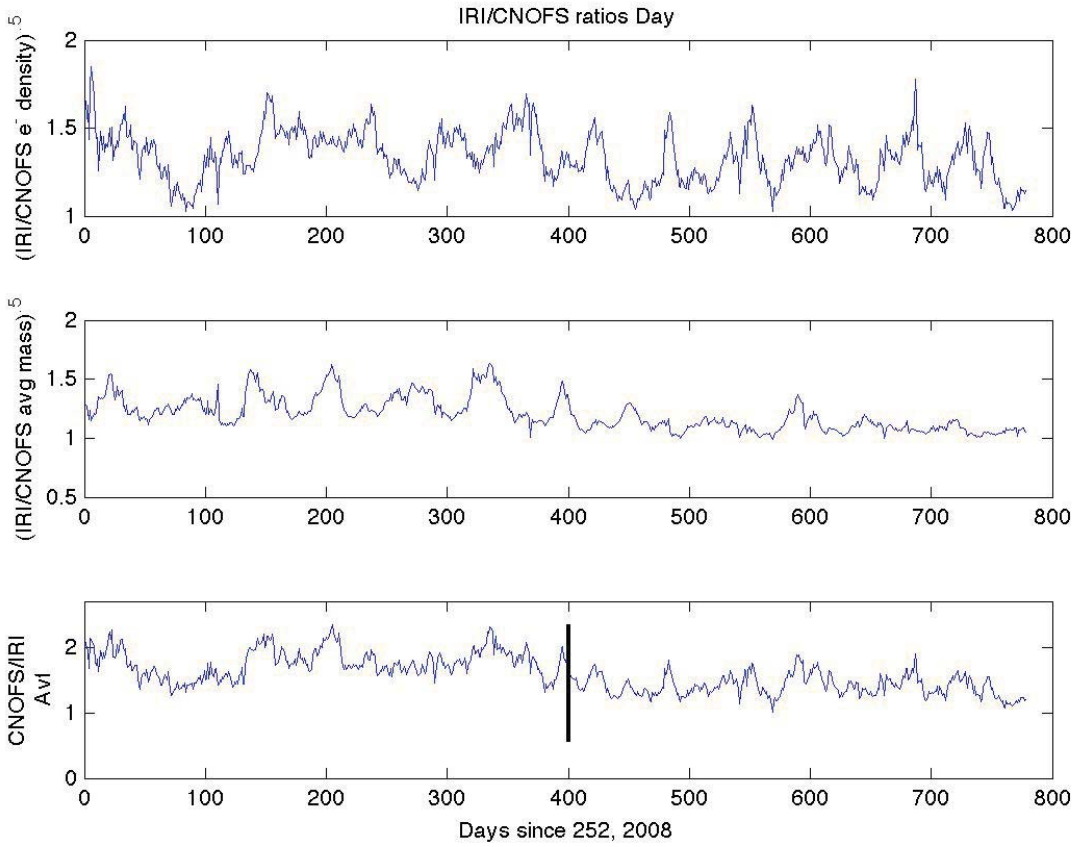

Figure 4: Same as figure 3 for daytime measurements only. The transition out of solar minimum can be seen at day 400.

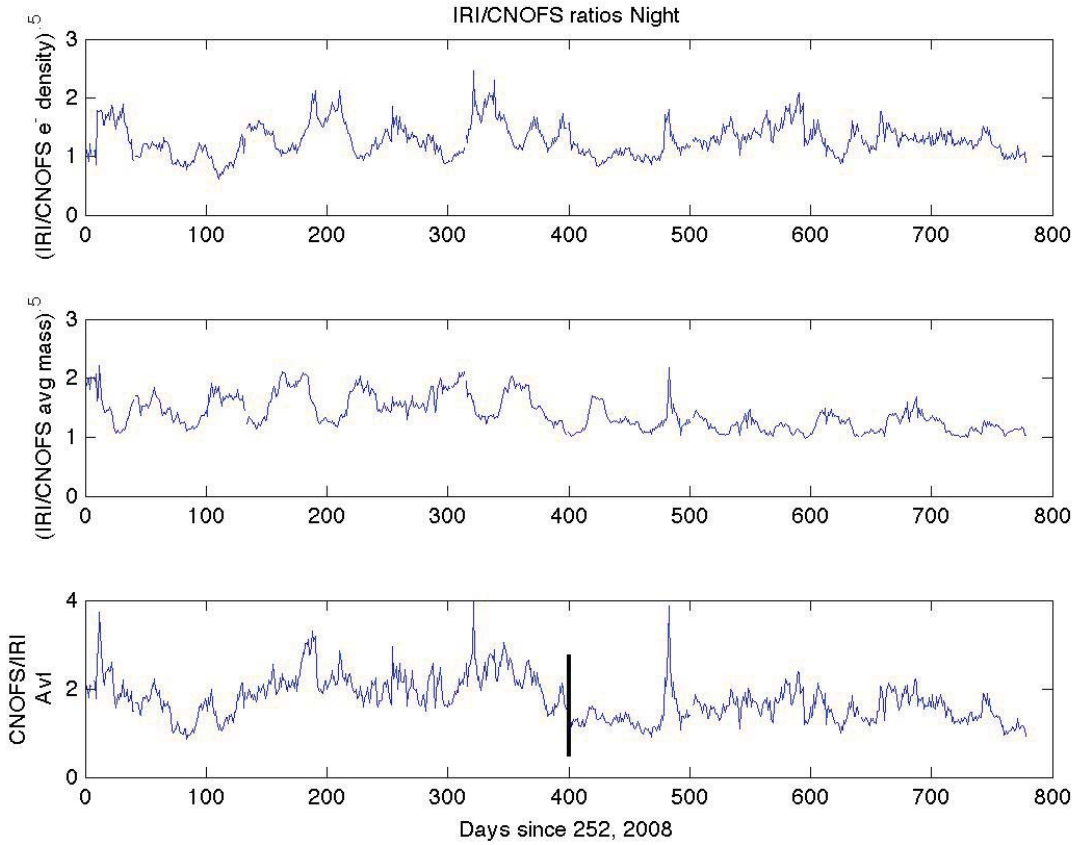

Figure 5: Same as figure 3 for nighttime measurements only. The transition out of solar minimum is evident after dav 400.

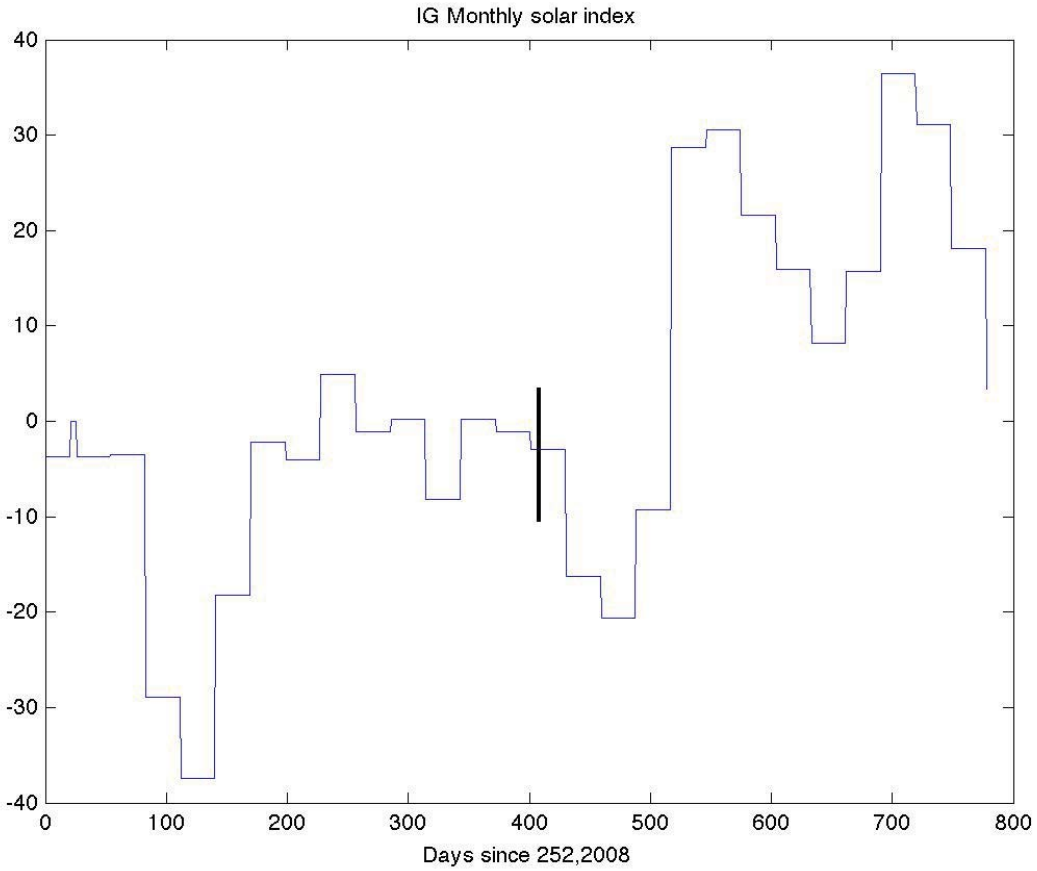

Figure 6: IG index variation through the mission. The IG monthly index is used by IRI in order to create ionospheric predictions. The transition out of solar minimum can be seen at day 400. There is also a minimum for the value around the time of the solar minimum, but it is relatively short and the subsequent values show a quick rise in activity followed by a plateau until the transition out of the solar minimum following day 400.

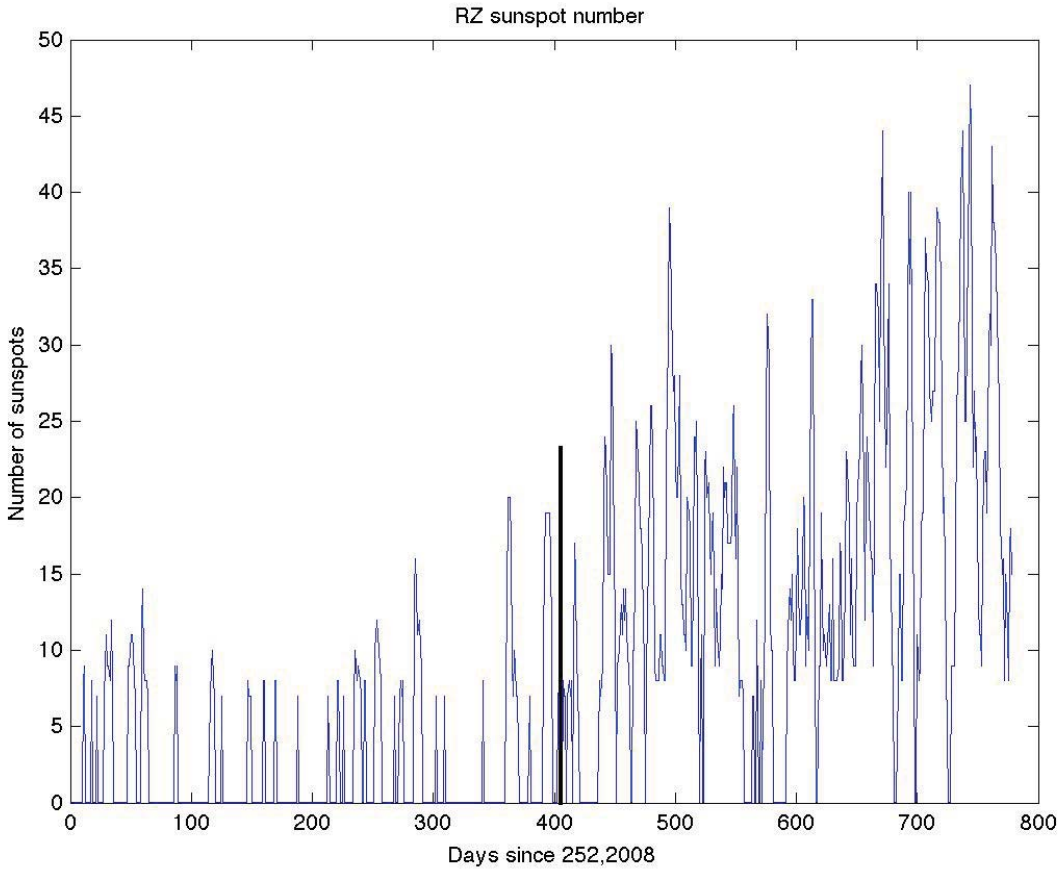

Figure 7: The figure shows the daily sunspot number. The plateau is observable before day 400, with the absolute minimum of zero sunspots being observed several times. After day 400, corresponding with the transition out of solar minimum, the RZ values pick up noticeably.

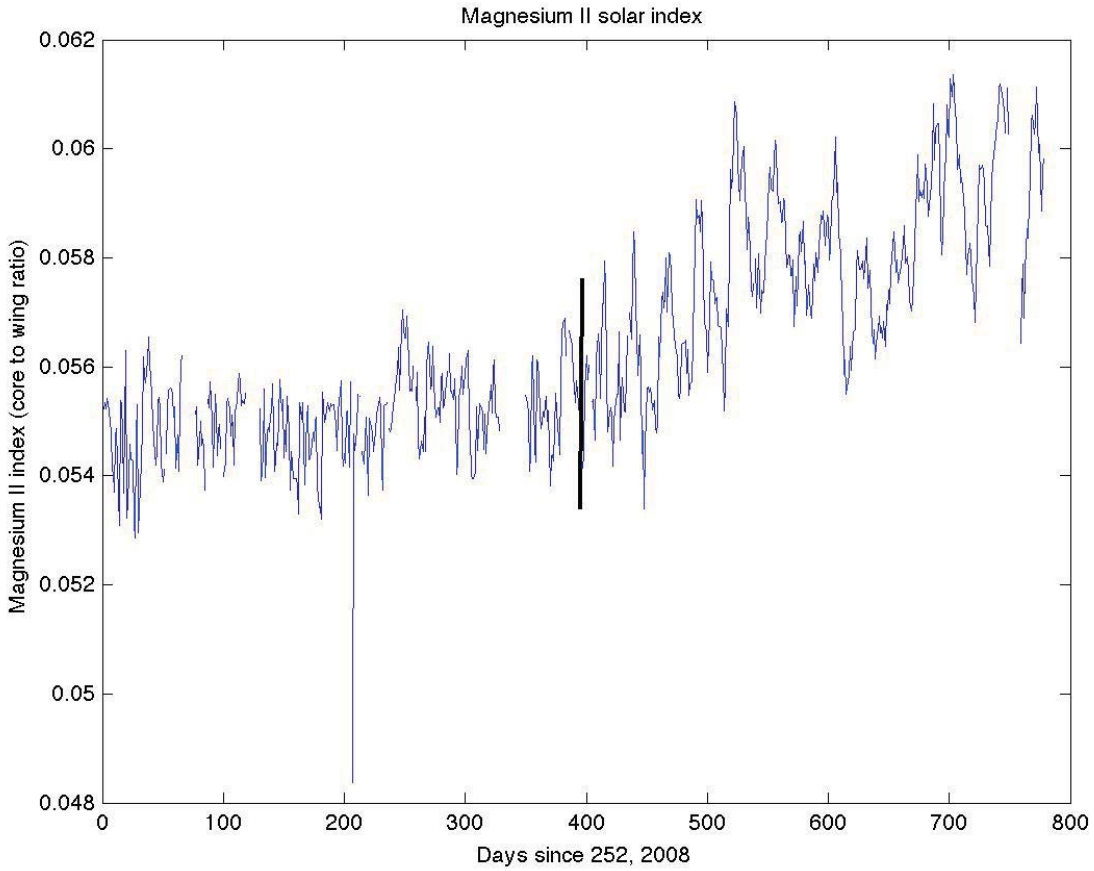

Figure 8: Magnesium II (280 nm) index as a function of mission time. The Magnesium II index shows a similar pattern to the RZ index, experiencing a plateau before picking up when transitioning out of the solar minimum.

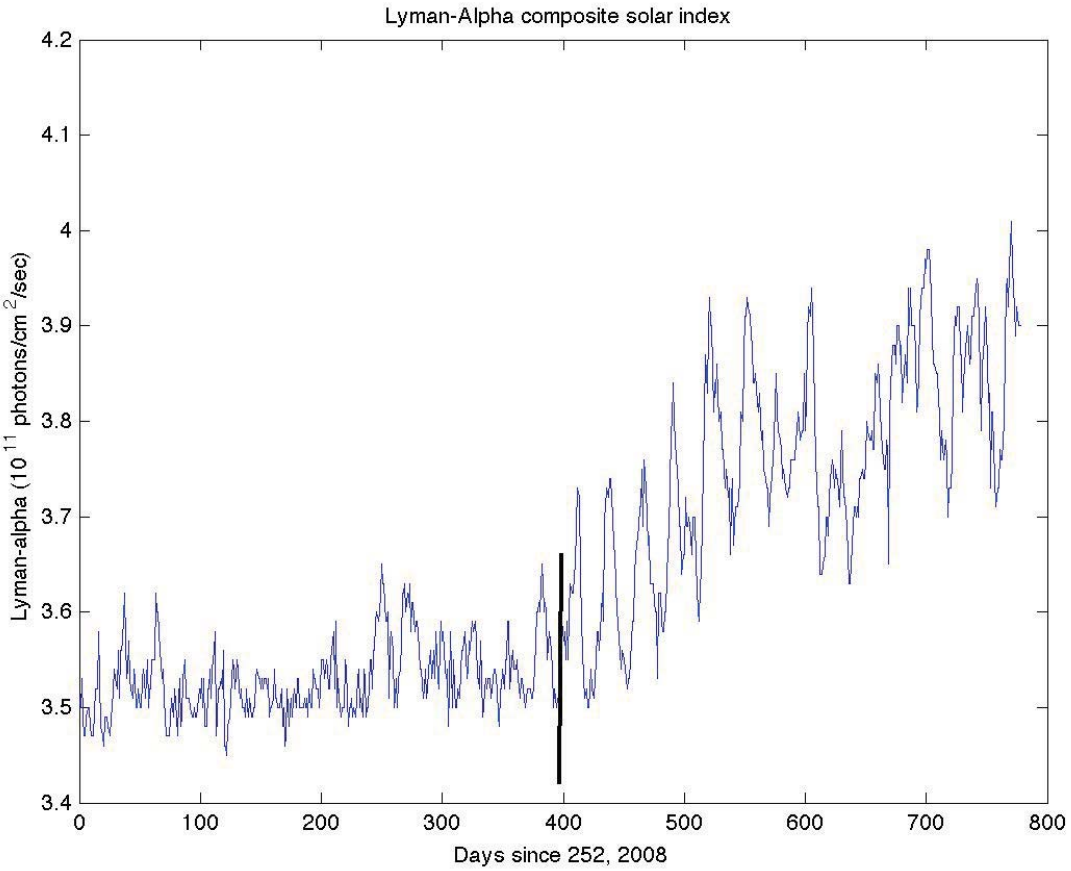

Figure 9: Lyman-Alpha (122 nm) composite solar index over the course of the mission. The pattern of the Lyman-Alpha index is similar to that of the Magnesium II index.

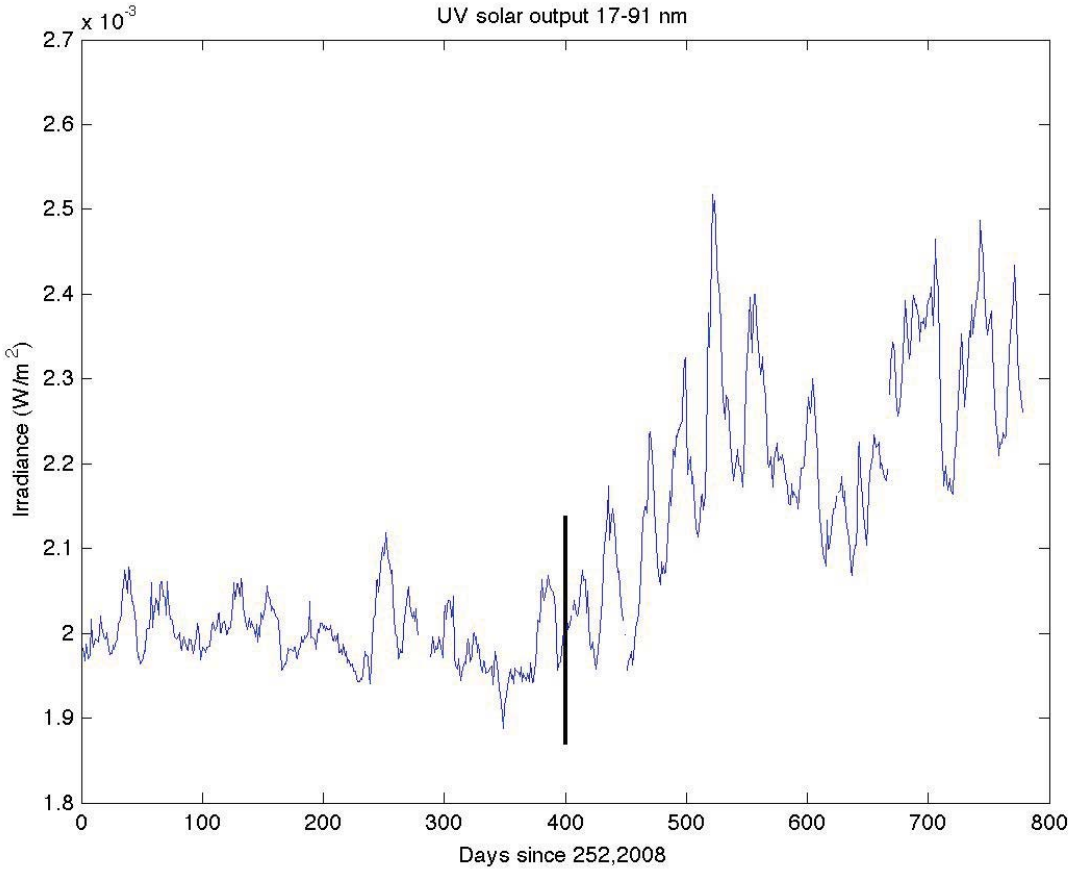

Figure 10: UV solar output in the bandwidth 17-91 nm through the mission. The UV solar output plot shows the same trend of plateau followed by increase after day 400 near the end of the solar minimum, this agrees with the RZ value trend and the Magnesium II trend.